Experimental study on ZnO-TiO₂ sorbents for the removal of elemental mercury

Kunzan Qiu, Jinsong Zhou[†], Pan Qi, Qixin Zhou, Xiang Gao, and Zhongyang Luo

State Key Laboratory of Clean Energy Utilization, Zhejiang University, Hangzhou 310027, P. R. China

Abstract−ZnO-TiO₂ sorbents synthesized by an impregnation method were characterized through XRD (X-ray diffraction), XPS (X-ray photoelectron spectroscopy) and EDS (Energy dispersive spectrometer) analyses. An experiment concerning the adsorption of Hg^0 by ZnO-TiO₂ under a simulated fuel gas atmosphere was then conducted in a bench-scale fixed-bed reactor. The effects of ZnO loading amounts and reaction temperatures on Hg^0 removal performance were analyzed. The results showed that ZnO-TiO₂ sorbents exhibited excellent Hg^0 removal capacity in the presence of H_2S at 150 °C and 200 °C; 95.2% and 91.2% of Hg^0 was removed, respectively, under the experimental conditions. There are two possible causes for the H_2S reacting on the surface of ZnO-TiO₂: (1) H_2S directly reacted with ZnO to form ZnS, (2) H_2S was oxidized to elemental sulfur (S_{ad}) by means of active oxygen on the sorbent surface, and then S_{ad} provided active absorption sites for Hg^0 to form HgS. This study identifies three reasons why higher temperatures limit mercury removal. First, the reaction between Hg^0 and H_2S is inhibited at high temperatures. Second, HgS, as the resulting product in the reaction of mercury removal, becomes unstable at high temperatures. Third, the desulfurization reaction strengthens at higher temperatures, and it is likely that H_2S directly reacts with ZnO, thus decreasing the S_{ad} on the sorbent surfaces.

Keywords: Mercury, ZnO-TiO₂, Removal Efficiency, H_2S, Simulated Gas

INTRODUCTION

China is currently undergoing a process of industrialization and urbanization that has significantly increased energy consumption. The use of coal for generating electricity is continuously growing and mercury pollution is worsening [1-3]. Based on test data that Hu et al. [4] estimated mercury emissions from coal-fired power plants in China, their results showed that total mercury emissions from coal plants in China were approximately 193.6 tons, including 147 tons of gaseous mercury. According to a UNEP report [5,6], approximately 40% of total worldwide mercury emissions come from China; coal burning is the primary emission source, accounting for 70% of all domestic anthropogenic mercury [7,8]. It is clear that traditional technologies of development and utilization are severely harming the economy and environment. To promote the coordination of development between energy, economic, environmental interests and reduce the causes of air pollution, it is crucially important to develop high-efficiency clean-coal technology [9].

Coal gasification technology has enormous potential; clean-coal technology is an important component in the integrated gasification combined cycle (IGCC) generation system [10,11]. Compared with traditional coal-burning technology, IGCC has many advantages, such as high efficiency, flexible raw material options, abundant byproducts, and low operational and maintenance costs [12,13]. However, coal gasification technology also creates problems concerning mercury pollution. During the gasification process, toxic trace elements of mercury are released at amounts even higher than in coal-fired flue gas [14], which is almost a zero-valence state. However, capturing Hg^0 is relatively difficult due to its low water solubility and high volatilization. In contrast, Hg^{2+} is freely soluble in water, and Hg_p is easily captured with a dust collector. For this reason, catalytic oxidation and adsorption are good methods for Hg^0 removal [15,16]. However, it has been demonstrated that environmental reductions are not achievable with Hg oxidation solely through gas phase reactions [17]. In addition, the mechanisms for the catalytic oxidation and absorption of mercury are still unclear, making it more difficult to remove Hg^0. Thus, more research concerning the removal of mercury from syngas is required.

The sorbents currently used for environmental mercury removal are still under study, and there are application problems that still need to be solved. Precious metals can be used to effectively remove Hg^0 from simulated fuel gas at temperatures of 204-288 °C by forming amalgams [18-20]. Nevertheless, unstable mercury removal efficiency (precious metals can be vulnerable to H_2S or HCl [21]) and high production costs seriously limit their industrial application. Active carbons (ACs), though one of the most widely used sorbents, are sensitive to temperature; above 150 °C, AC performance rates for mercury removal rapidly decline [22]. Iron oxide, as a desulfurization sorbent for hot coal gas, exhibits superior mercury absorption ability with the aid of H_2S. Under an Eley-Rideal mechanism, H_2S is selectively oxidized to elemental sulfur (S_{ad}) on iron-based sorbents; the adsorbed S_{ad} then reacts with Hg^0 to form stable HgS. However, this mechanism is also significantly influenced by high temperatures, with optimal mercury removal achieved at approximately 150 °C [23]. In most industrial gasification processes, temperatures range near 200 °C after water quench cleaning, including the Shell and Texaco gasification processes [24]. There-

fore, the temperature we must consider for mercury removal is 200 °C to ensure gasification thermal efficiency.

TiO$_2$ sorbents and Nano-ZnO sorbents have been widely used for coal gasification desulfurization. Mn-TiO$_2$ catalyst [25] can remove elemental mercury up to 95% at 300 and 350 °C from flue gas. Reddy et al. [26,27] reported that MnO$_x$/CeO$_2$-TiO$_2$ catalysts showed effective adsorbents for removing elemental mercury from flue gas at 175-200 °C, and the mechanism for Hg adsorption over Mn-Ce-Ti sorbents has no connection of the presence of SO$_2$. In an earlier study [28], adsorption tests of elemental mercury with nano-ZnO under a simulated gas atmosphere were evaluated in a bench-scale fixed-bed apparatus, and some progress was reported. Nevertheless, a significant disadvantage of nano-ZnO sorbents was that their optimum mercury removal temperature was 80 °C. In this work, Zn-Ti-based sorbents were prepared by an impregnation method to remove mercury in the presence of H$_2$S at higher temperatures. The effects of temperature and sorbent composition were investigated. The possible reasons for high temperature inhibiting Hg^0 removal efficiency were proposed and confirmed through XPS characterization and TPD experiments.

EXPERIMENTAL SECTION

1. Sample Preparation and Characterization

Different mass ratios of ZnO-TiO$_2$ were prepared with an impregnation method using TiO$_2$ nanoparticles as supports. Dried TiO$_2$ was added to certain concentrations of zinc nitrate solution. The mixtures were continuously stirred for 2 h, dried at 120 °C for 3 h and then calcined in a muffle kiln at 500 °C for 3 h. The samples were crushed and sieved through an 80-mesh screen (180 μm). For convenience, the samples are denoted as Zn-Tix, where Zn represents ZnO, Ti represents TiO$_2$, and x, in the range of 0.02 to 1, represents the mole ratio of ZnO/TiO$_2$.

The crystal species distribution of the sorbents was determined by X-ray diffraction (an X'Pert PRO system). The morphology of the samples was determined with a field emission scanning electron microscope (JSM-6390LA). XPS analysis was conducted to determine the surface elemental concentration of materials (thermo ESCALAB MARK II).

2. Apparatus and Procedure

The Hg^0 removal activities of ZnO-TiO$_2$ in the simulated syngas were investigated with the bench-scale fix-bed reactor system shown in Fig. 1. The entire system consisted of five parts: a simulated syngas supply system, a mercury vapor generator, an adsorption reactor, a gas analysis system and an exhaust gas purge system.

The total gas flow rate was 1 L/min, and another 200 mL/min of N$_2$ was passed through a temperature-controlled mercury permeation tube (VICI Metronic, Inc. U.S.A.) to generate a constant rate of Hg^0 (~50 μg/m^{-3}). The gas components were mixed at 1.2 L/min and preheated to a certain temperature and then diverted from the reactor. The concentrations of Hg^0 and Hg^{2+} in the mixed gas were continuously measured with a DM-6A/MS-1A mercury analyzer (Nippon Inc. Japan). After the system exhibited stable mercury feeding, the mixed gas was reverted to the reactor by turning
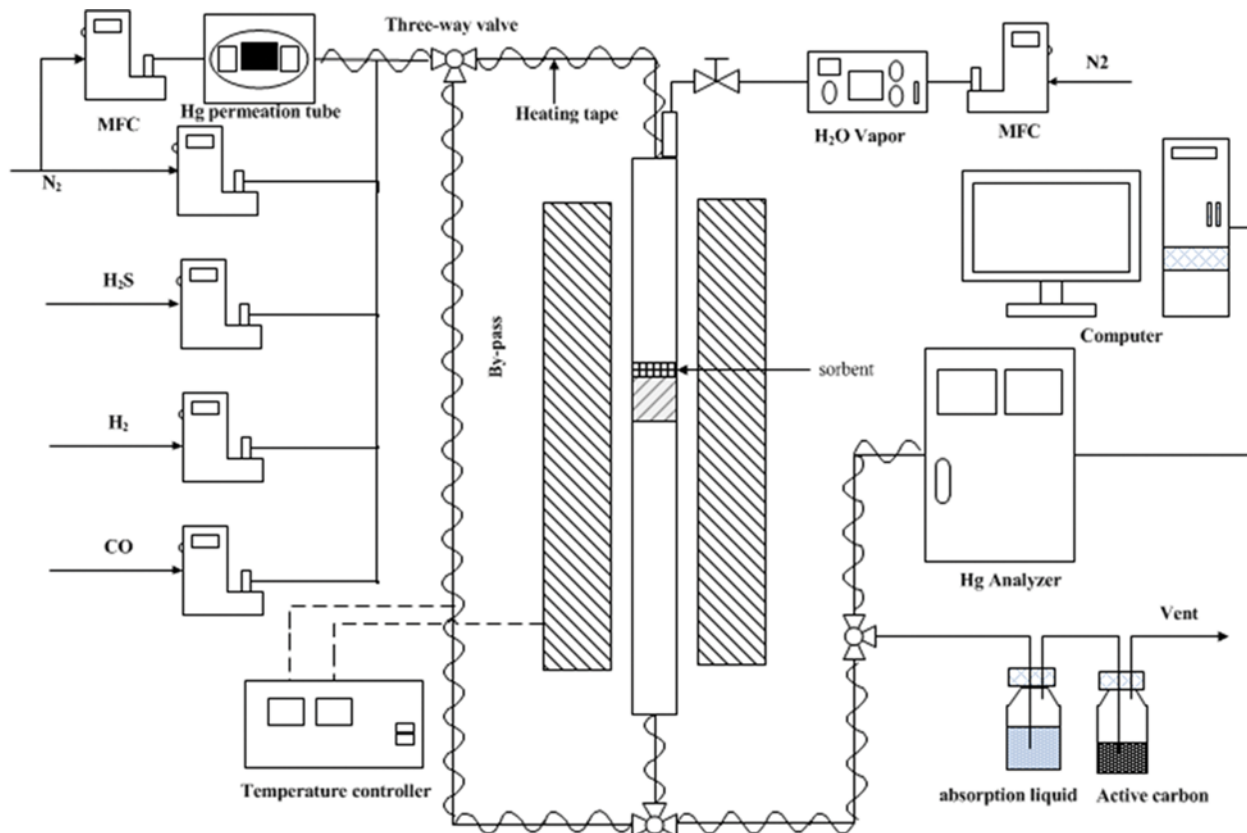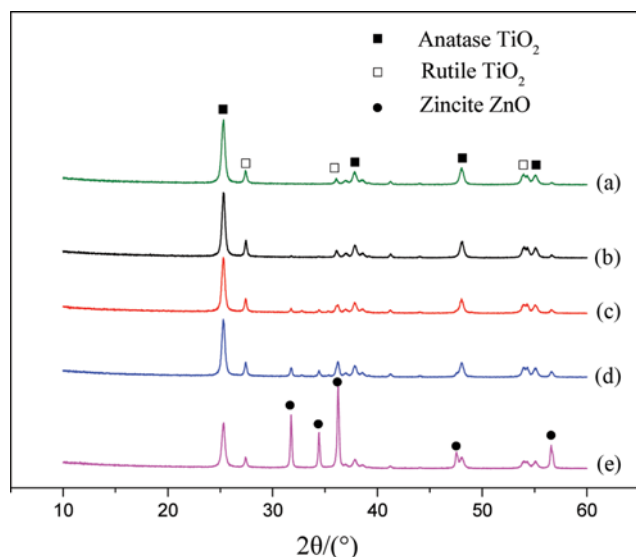

Fig. 1. Fixed-bed reaction system.

Fig. 2. XRD pattern of the Zn-Tix ((a) TiO$_2$, (b) Zn-Ti 0.02, (c) Zn-Ti 0.1, (d) Zn-Ti 0.2, (e) Zn-Ti 1).

Table 1. Energy spectrum analysis of sorbents

	Element	Mass%	Atomic%
Zn-Ti 0.02	O	34.57	61.50
	Ti	63.10	37.49
	Zn	02.32	01.01
Zn-Ti 0.1	O	34.39	61.78
	Ti	58.42	35.05
	Zn	07.19	03.16
Zn-Ti 0.2	O	35.79	63.45
	Ti	54.92	32.52
	Zn	09.29	04.03
Zn-Ti 1	O	30.41	58.85
	Ti	47.35	30.61
	Zn	22.24	10.54

the three-way valve and passing through the sorbent. The mass of the sample for each measurement was 0.2 g, and the exhaust gas emissions were purified by an absorption device filled with activated carbon.

Negligible Hg^{2+} was observed in each test; therefore, the decrease in Hg^0 concentration across the sorbent was attributed to Hg^0 absorption. Thus, the elemental mercury removal efficiency (η) over ZnO-TiO$_2$ can be defined as follows:

$$\eta = (c_{in} - c_{out})/c_{in} \times 100\% \qquad (1)$$

where, c_{in} and c_{out}, in $\mu g/m^3$, represent the inlet and outlet Hg^0 concentrations, respectively.

RESULTS AND DISCUSSION

1. Characterization of Sorbents

The XRD spectra of different ZnO loading samples are shown in Fig. 2, where it can be concluded that both anatase TiO$_2$ and rutile TiO$_2$ were detected. By comparing the two types of TiO$_2$ spectra peaks, the diffraction intensity of the anatase TiO$_2$ was obviously stronger than the rutile, meaning that the anatase TiO$_2$ was the dominant phase. When the ZnO content on the TiO$_2$ was insufficient, it was difficult to determine the ZnO diffraction peaks. This implies that ZnO was either highly dispersed over the TiO$_2$ or existed in small particles. When the mole ratio of ZnO/TiO$_2$ increased, the diffraction line of ZnO became more apparent, suggesting that ZnO crystallites were formed; when the ratio is less than 0.2, the ZnO was highly dispersed.

The surface elemental analysis of sorbents performed with EDS is shown in Table 1. We can easily conclude that the relative content of ZnO on TiO$_2$ increased when the mole ratio of ZnO/TiO$_2$ increased, which concurs with the conclusion from XRD and indicates that ZnO was highly dispersed on TiO$_2$.

2. Effect of ZnO Loading Amount

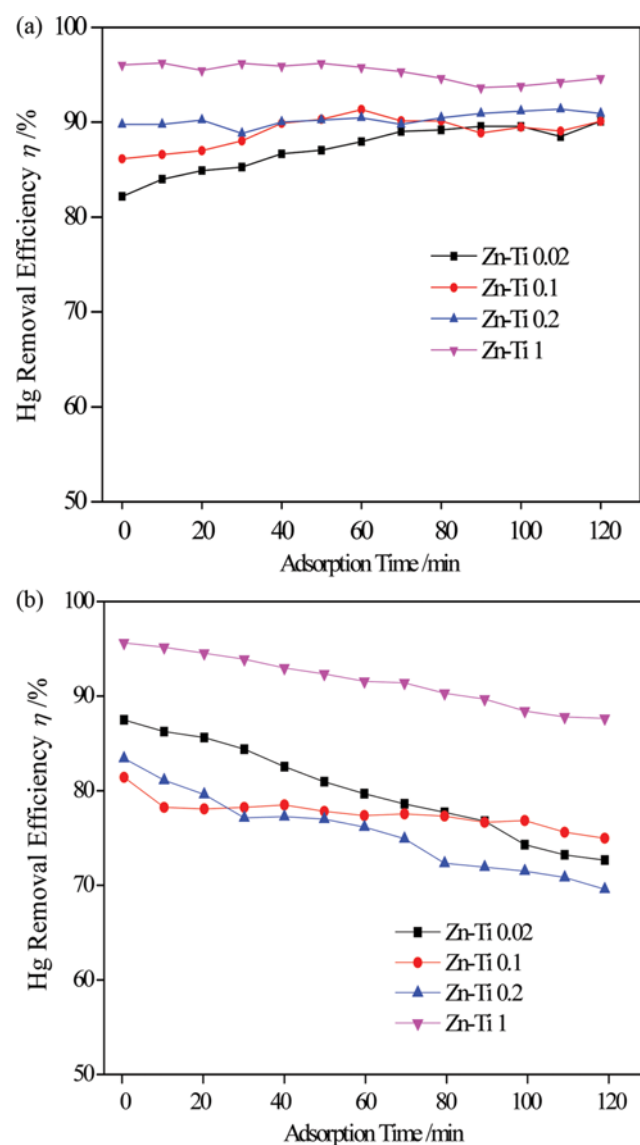In the preliminary experiments, Hg^0 was barely adsorbed by Zn-

Fig. 3. Hg removal efficiency of Zn-Tix composite adsorbent in N$_2$+400 ppm H$_2$S ((a) 150 °C, (b) 200 °C).

Table 2. The physical structure of the sorbents surface

| Sample	Surface area (m^2/g)	Pore volume (m^3/g)	Average pore size (nm)
Zn-Ti 0.02	40.8866	0.364	35.579
Zn-Ti 0.1	37.6407	0.351	37.342
Zn-Ti 0.2	20.9132	0.240	45.891
Zn-Ti 1	7.4161	0.117	63.004

Tix in a pure N_2 atmosphere at either 150 °C or 200 °C. This indicates that ZnO-TiO_2 has a poor physical adsorption capacity. To examine the atmospheric chemi-adsorption of mixed metallic oxide sorbents, different ratios of ZnO-TiO_2 were used to remove Hg^0 in a N_2 atmosphere with 400 ppm H_2S at 150 °C and 200 °C; the results are shown in Fig. 3.

As seen in the figure above, mercury removal efficiency was markedly improved when H_2S was added, which agrees with previous research [29]. Because the elemental sulfur in the H_2S is in a reduced state, direct oxidation of mercury becomes difficult and a homogeneous oxidation reaction between H_2S and Hg^0 seldom occurs. It can thus be deduced that the removal of Hg with H_2S depends on a heterogeneous reaction. H_2S in the simulated gas can be oxidized by ZnO-TiO_2 to elemental sulfur (S_{ad}); Hg^0 can be oxidized by elemental sulfur to form HgS deposited over the surface [30].

At 150 °C, a higher mole ratio of ZnO/TiO_2 showed higher Hg^0 removal efficiency; the effects of increasing ZnO loading can be summarized by two aspects. First, as shown in Table 2, the BET surface area decreased with increased ZnO loading, reducing the physical adsorption capacity of ZnO-TiO_2. Second, more ZnO doped on TiO_2 samples leads to better chemical adsorption properties. Chemi-adsorption was dominant at 150 °C; higher ZnO loading generated more active elemental sulfur, thus improving Hg^0 removal efficiency. When the reaction temperature reached 200 °C, the value h decreased with increased ZnO loading from 0.02 to 0.2 and then increased significantly as the mole ratio of ZnO/TiO_2 increased to 1. Until the mole ratio of ZnO/TiO_2 reached 0.2, the physical adsorption capacity of H_2S reduced with decreasing BET surface area and chemical adsorption improved, causing an unfavorable condition for Hg^0 absorption and oxidation. As a result, Hg^0 removal efficiency decreased as a matter of course. Further increasing the ratio significantly enhanced the chemisorption of H_2S, making up for the insufficient physisorption. Consequently, the value of h increased again. This was confirmed in the EDS test results; the zinc content of the first three ratios was below 10%, whereas the content of zinc in ZnTi1 reached 22%, making it possible to significantly improve chemisorption. In conclusion, Zn-Ti1 is the most suitable sorbent in four different ratios. At 150 °C and 200 °C, Hg removal efficiency reached 95.2% and 91.2%, respectively. This implies that the effective mercury removal temperature was significantly raised. As a result, ZnTi1 was selected as the research subject in the following tests.

3. Effect of Temperature

To investigate the temperature effect on the performance of Zn-Ti1 in the presence of N_2 and 400 ppm H_2S, mercury removal re-
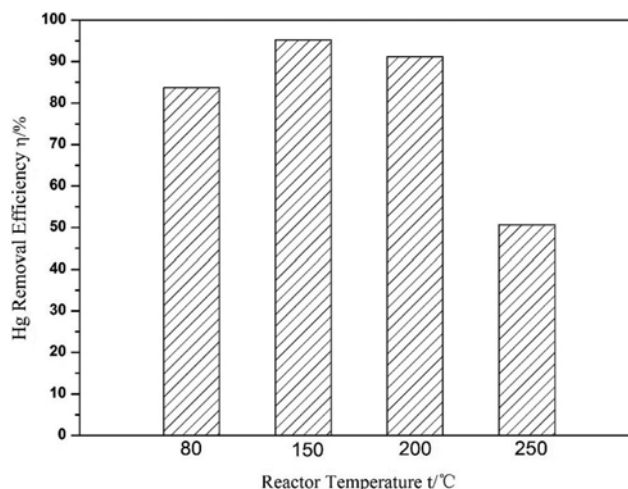
Fig. 4. Effect of temperature on Hg^0 removal on ZnTi1 in N_2+400 ppm H_2S.

search was conducted at 80 °C, 150 °C, 200 °C and 250 °C. As shown in Fig. 4, Hg^0 removal efficiency initially increased and subsequently decreased with increasing temperature. The maximum value of η appeared at 150 °C, with an adsorption efficiency of 95.2%. When the temperature reached 200 °C, the efficiency dropped slightly to 91.2%. In addition, the performance of the Zn-Ti1 sorbents dramatically deteriorated at 250 °C and the value η fell to 50.7%. Hg^0 removal efficiency was fairly stable within 2 h below 200 °C. In contrast, the efficiency decreased over time above 200 °C. Elevated temperature contributes to the process of chemi-adsorption, promoting the chemical reaction of H_2S over the surface of sorbents. Nevertheless, it impedes the physisorption of adsorbates over the surface.

4. Desorption Characteristic of Mercury Species

To obtain more detailed information on the characteristics of mercury captured on ZnO-TiO_2, a temperature programmed decomposition (TPD) technique was applied in the same fixed-bed reactor. As shown in Fig. 5, sorbents used for 2 h of Hg^0 removal experiments at 200 °C and 8 h of experiments at 150 °C were selected to consider the influence of temperature. To avoid the peak value exceeding the measurement range, only 800 mg of mercury-absorbed samples were packed in the quartz tube reactor and N_2 flowed through the reactor at a rate of 1 L/min as a protective atmosphere. The sample was then heated from 50 °C to 400 °C at a heating rate of 10 °C/min.

The combined Hg adsorbed on the sorbents can be recovered as elemental mercury. In comparing the two curves, that the mercury desorption peaks of ZnO-TiO_2 sorbent appeared between 250-270 °C. A similar temperature range of Hg desorption peaks in HgS was obtained by WU et al. [30,31]. The above results prove that absorbed mercury primarily exists in the form of HgS on the surface of Zn-Ti1 and that HgS is unstable and easily decomposes at approximately 250 °C, thus revealing a possible reason for low Hg^0 removal efficiency at elevated temperatures. The possible pathway responsible for Hg desorption is shown below: [32]
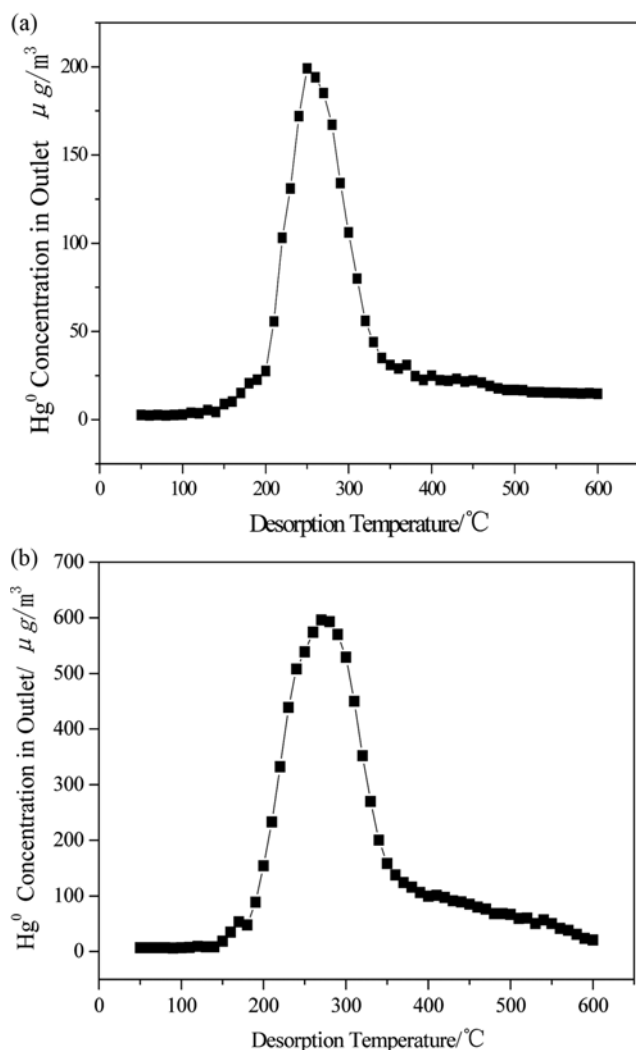
$$HgS \rightarrow Hg^0 + (1/x) S_x \qquad (2)$$

Fig. 5. Temperature programmed decomposition desorption (TPD) spectra of mercury species-adsorbed Zn-Ti1 sorbents ((a) temperature: 150 °C length of time: 8 h, (b) temperature: 200 °C length of time: 2 h).

Fig. 6. XPS spectra of O 1s for Zn-Ti1 samples ((a) fresh, (b) after Hg⁰ adsorption at 150 °C, (c) after Hg⁰ adsorption at 250 °C).

Table 3. The thermodynamic parameters of the reaction between S and Hg [32]

Temperature (°C)	S(s)+Hg(g)→HgS(s)	
	ΔG (kJ/mol)	K
50 °C	−79.6	7.45×10^{12}
120 °C	−71.5	3.13×10^{9}
160 °C	−66.8	1.15×10^{8}
200 °C	−62.3	7.55×10^{6}
250 °C	−58.1	6.38×10^{5}

Further investigation is required to clarify other possible forms of mercury compounds and other pathways for decomposition.

Table 3 shows the thermodynamic parameters of the reaction between sulfur and mercury. In Table 3, the reaction is exothermic, and the equilibrium spontaneously shifts toward the right at lower temperatures. As the temperature rises, the equilibrium constant K
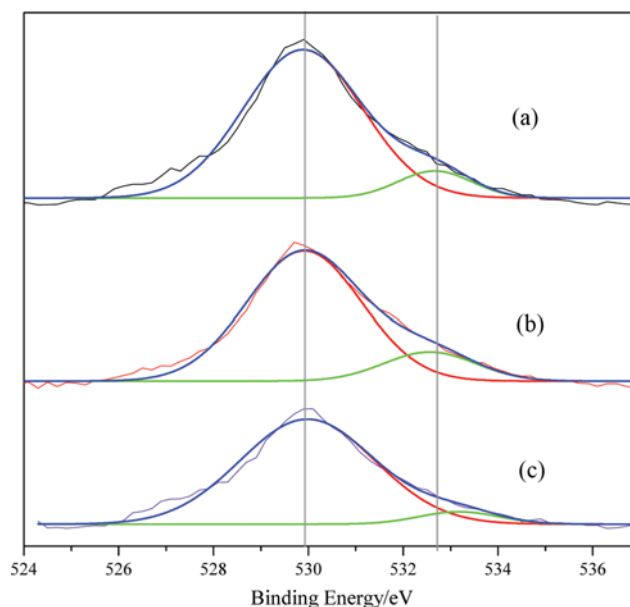
decreases sharply, and the reaction between Hg⁰ and S is inhibited; the equilibrium of the reaction shifts toward the decomposition reaction of HgS, drastically decreasing the HgS concentrations. This is the reason that Hg⁰ removal efficiency drops once the temperature rises above 150 °C.

5. Surface Analysis and Reaction Mechanism

Active oxygen absorbed on zinc-based sorbents plays an important role in the mercury removal process. To further study the changes of oxygen with adsorption temperature, XPS spectra were conducted for oxygen on the surface of the sorbents before and after mercury removal tests at 150 °C and 250 °C. The results are shown in Fig. 6. The O 1s spectra of Zn-Ti1 included two peaks. The peak at approximately 530.0 eV was assigned to lattice oxygen, while the other, with a higher binding energy value, was attributed to chemisorbed oxygen or other oxygenic substances in the weak absorption condition.

As shown in Fig. 6, the relative content of chemisorbed oxygen on the samples after Hg⁰ adsorption was greater than the untreated sample at 150 °C. This indicates that some of the lattice oxygen transformed into absorbed oxygen during the Hg and H₂S adsorption process with the TiO₂ catalyst, thus offsetting the consumption of absorbed oxygen; this was consistent with a previous report on absorbing Hg⁰ with V₂O₅/TiO₂ [33]. In this situation, there was sufficient active absorbed oxygen on the ZnO-TiO₂ to stably adsorb H₂S, and the mercury removal efficiency remained stable. Conversely, the relative content of chemisorbed oxygen on the sorbents declined sharply at 250 °C and the O 1s peaks shifted slightly to a higher binding energy. In considering the noticeable H₂S removal capacity of ZnO at 250 °C, the possible reaction is shown as Eq. (3). ZnO reacted with H₂S to form H₂O, as weakly bound oxygen, on the surface of the Zn-Ti1 and mixed with chemisorbed oxygen to cause the peak shift. In addition, the reactions between Hg and H₂S were stronger at 250 °C, and some lattice oxygen was
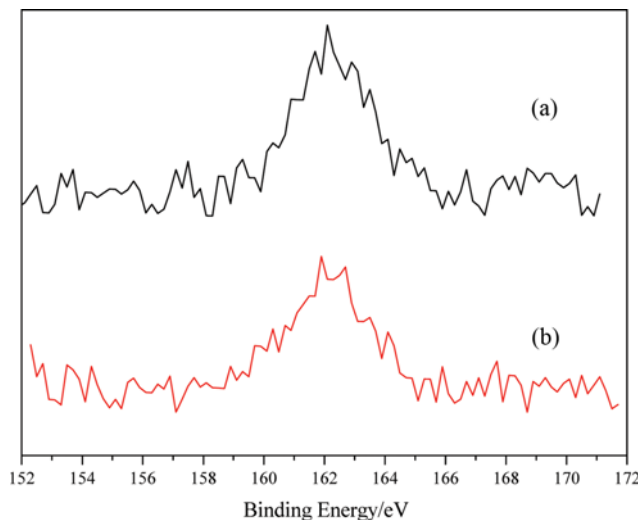
Fig. 7. XPS spectra of S 2p for Zn-Ti1 samples after Hg^0 adsorption ((a) at 150 °C, (b) at 200 °C).

Fig. 8. XPS spectra of Zn 2p for Zn-Ti1 samples ((a) fresh, (b) after Hg^0 adsorption at 150 °C, (c) after Hg^0 adsorption at 250 °C).

replaced by S^{2-}, decreasing the transformational amount of lattice oxygen to absorbed oxygen. As the experiment progressed, the amount of absorbed oxygen gradually declined, and Hg^0 removal efficiency decreased over time.

XPS spectra were also obtained for sulfur on the surface of the sorbents after absorbing Hg^0 at 150 °C and 200 °C; the results are shown in Fig. 7. The main peaks were both observed at 162.1 ev; this indicates that S likely existed as HS, in the form of polysulfide, on the ZnO-TiO$_2$ sorbent surface. In comparing the XPS spectra after tests at different temperatures, the shoulder peaks at approximately 164.5 ev of the samples after Hg^0 adsorption at 150 °C were wider than those at 200 °C, and the peaks of the former at approximately 161 ev were lower than those of the latter. It is likely that the S^0 content on the surface of the Zn-Ti1 absorbing Hg^0 at 150 °C was greater than the S^{2-} content. This indicates that, at 250 °C, more lattice oxygen was replaced by S^{2-}, and the S^{2-} generated by the direct reaction between H$_2$S and ZnO was more difficult to oxidize into S^0. This may also help to explain why efficiency was lower at 250 °C. Another phenomenon deserves mention: with the increase of temperature, the samples after Hg^0 adsorption were darker. For example, the sorbent that absorbed mercury at 150 °C was pale yellow, whereas the sorbent at 200 °C was light grey. This means the reaction product was affected by temperature.

XPS spectra were then conducted for zinc on the surface of the sorbents before and after Hg^0 removal at 150 °C and 200 °C; the results are shown in Fig. 8. We found that (1) the Zn 2p peaks changed little after absorbing H$_2$S and Hg at 150 °C, and (2) the Zn 2p peaks shifted slightly to a lower binding energy at 250 °C. With increasing temperature, the reaction between ZnO and H$_2$S became move violent, and some lattice oxygen was replaced by S^{2-}, thus forming a chemical bond between Zn and S. Because the electronegativity of a sulfur atom is lower than that of an oxygen atom, the electron density around the zinc atom changed. Similarly, the Ti 2p peaks did not obviously change after experiments at 150 °C, whereas the peaks were enhanced at 250 °C. It is likely that the state of the titanium was influenced by the change in the zinc atom. We
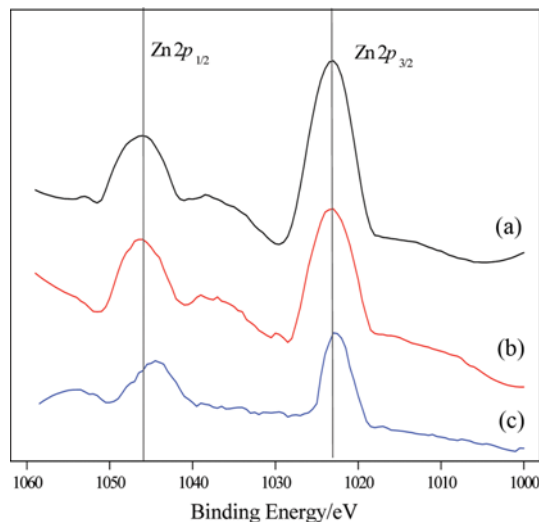
conclude that the likelihood of zinc participating in the reaction increases at 250 °C, thus enhancing the desulfurization of the zinc-based sorbent.

Based on the experimental results above, we can summarize the reactions between Hg^0 and H$_2$S on ZnO-TiO$_2$ as follows: ZnO reacts with H$_2$S to produce ZnS and the lattice oxygen is replaced. In addition, H$_2$S is oxidized to S$_{ad}$ by the catalytic oxidation effect of active oxygen on the surface of the sorbent; Hg^0 then reacts with S$_{ad}$ to form HgS, effectively removing mercury. Thus, in the presence of H$_2$S, the following reactions should be proposed as the overall reactions on the ZnO-TiO$_2$ sorbent:

$$H_2S(g) + ZnO \rightarrow ZnS + H_2O \tag{3}$$

$$H_2(g) + O^* \rightarrow S_{ad} + H_2O \tag{4}$$

$$S_{ad} + Hg^0 \rightarrow HgS \tag{5}$$

CONCLUSIONS

Zn-Ti1 sorbents exhibited high Hg^0 removal capacity in the presence of H$_2$S at 150 °C and 200 °C, and the efficiency h reached 95.2% and 91.2%, respectively. Thus, further increasing the temperature at which mercury can be effectively absorbed by zinc-based sorbents under simulated coal-derived fuel gas. This study revealed two major possible reactions that H$_2$S enabled on the surface of ZnO-TiO$_2$. First, ZnS was produced by the reaction between H$_2$S and ZnO, placing lattice oxygen onto the surface of the zinc-based sorbents. Second, H$_2$S was oxidized to S$_{ad}$ by the aid of active oxygen, and S$_{ad}$ then provided active absorption sites for Hg^0 to form HgS. We determined that higher temperatures inhibited mercury removal for the following reasons: (1) the reaction between Hg^0 and H$_2$S was inhibited at high temperatures, inducing a decrease in HgS, (2) HgS, as a reaction product in mercury removal, became unstable at high temperatures, and (3) the desulfurization reaction became stronger at high temperatures. It is likely that H$_2$S directly reacted with ZnO, thus decreasing the S$_{ad}$ on the surface of the sorbents.

ACKNOWLEDGEMENTS

REFERENCES

1. BP p.l. c. Statistical Review of World Energy 2013[R] (2013).
2. J. P. Longwell, E. S. Rubin and J. Wilson, *Prog. Energy Combust. Sci.*, **21**(4), 269 (1995).
3. J. S. Gary and C. M. Russell, *Fuel Process. Technol.*, **71**(1-3), 79 (2001).
4. C.-x. Hu, J.-s. Zhou, S. He, Z.-y. Luo and K.-f. Cen, *Thermal Power Generation*, **39**, 1 (2010).
5. UNEP. Report of the global mercury assessment working group on the work of its first meeting[R]. Geneva: UNEP (2002).
6. UNEP. Global Mercury Assessment 2013: Sources, Emissions, Releases, and Environmental Transport[R]. Geneva: UNEP (2013).
7. E. Sasmaz and J. Wilcox, *J. Phys. Chem.* C **112**, 16484 (2008).
8. J.-K. Jiang, J.-m. Hao, Y. Wu, G. S. David, L. Daun and H.-z. Tian, *Environ. Sci.*, **26**, 34 (2005).
9. Y.-f. Duan, L. Liu, H.-j. Wang, J.-j. Yin and C.-s. Zhao, *J. Taiyuan University of Technol.*, **41**, 619 (2010).
10. A. Licata and W. Fey, Advanced technology to control mercury emissions[C] EPA-DOEEPRI MEGA Symposium, Arlington Heights (2001).
11. D. Y. Lu, D. L. Granatstein and D. J. Rose, *Ind. Eng. Chem. Res.*, **43**(17), 5400 (2004).
12. J. Wilcox, Carbon Capture[M], Springer (2012).
13. J. H. Pavlish, L. L. Hamre and Y. Zhuang, *Fuel*, **89**, 838 (2010).
14. G. J. Stiegel and R. C. Maxwell, *Fuel Process. Technol.*, **71**, 79 (2001).
15. H. Zhang, J. Zhao, Y. Fang, J. Huang and Y. Wang, *Energy Fuels*, **26**, 1629 (2012).
16. Q.-c. Liu, W. Gao, C.-f. Lu and L.-y. Dong, *Gas&Heat*, **29**, 6 (2009).
17. A. Suarez Negreira and J. Wilcox, *Energy Fuels*, **29**, 369 (2014).
18. J. H. Pavlish, E. A. Sondreal, M. D. Mann, E. S. Olson, K. C. Galbreath, D. L. Laudal and S. A. Benson, *Fuel Process. Technol.*, **82**, 89 (2003).
19. E. J. Granite, C. R. Myers, W. P. King, D. C. Stanko and H. W. Pennline, *Ind. Eng. Chem. Res.*, **45**, 4844 (2006).
20. S. Aboud, E. Sasmaz and J. Wilcox, *Main Group Chemistry*, **7**, 205 (2008).
21. E. Sasmaz, S. Aboud and J. Wilcox, *J. Phys. Chem. C*, **113**, 7813 (2009).
22. D. B. Aeschliman and G. A. Norton, *Environ. Sci. Technol.*, **33**, 2278 (1999).
23. D. J. Couling, H. V. Nguyen and W. H. Green, *Fuel*, **97**, 783 (2012).
24. W.-h. Hou, J.-s. Zhou, Y. Zhang, X. Gao, Z.-y. Luo and K. Cen, *Proceedings of the CSEE*, **33**, 92 (2013).
25. J. Xie, N. Yan, S. Yang, Z. Qu, W. Chen, W. Zhang, K. Li, P. Liu and J. Jia, *Res. Chem. Intermed.*, **38**, 2511 (2012).
26. J. He, G. K. Reddy, S. W. Thiel, P. G. Smirniotis and N. G. Pinto, *J. Phys. Chem. C*, **115**, 24300 (2011).
27. G. K. Reddy, J. He, S. W. Thiel, N. G. Pinto and P. G. Smirniotis, *J. Phys. Chem. C*, **119**, 8634 (2015).
28. S. Wu, M. Azharuddin and E. Sasaoka, *Fuel*, **85**, 213 (2006).
29. J.-S. Zhou, Q. Pan, W.-h. Hou, S.-l. You, X. Gao and Z.-y. Luo, *J. Fuel Chem. Technol.*, **41**, 1371 (2013).
30. M. Ozaki, M. A. Uddin, E. Sasaoka and S. Wu, *Fuel*, **87**, 3610 (2008).
31. S. Wu, Md. A. Uddin, S. Nagano, M. Ozaki and E. Sasaoka, *Energy Fuels*, **25**, 144 (2010).
32. W. Liu, R. D. Vidic and T. D. Brown, *Environ. Sci. Technol.*, **34**, 154 (1999).
33. S. He, J. Zhou, Y. Zhu, Z. Luo, M. Ni and K. Cen, *Energy Fuels*, **23**, 253 (2009).